

Maps of Nonadiabatic Coupling in Triatomic Hydrogen

Ulrich Galster, Ulrich Müller, and Hanspeter Helm

*Department of Molecular and Optical Physics, Albert-Ludwigs-Universität,
Hermann-Herder-Strasse 3, D-79104 Freiburg, Germany*

(Received 18 July 2003; published 19 February 2004)

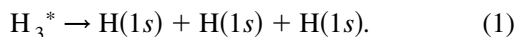
We show in an experiment that dissociation of state-selected neutral H_3^* molecules into three ground-state hydrogen atoms reveals highly structured maps of correlation in the motion of the three atoms. These maps provide a direct view of the internal molecular couplings which initiate dissociation.

DOI: 10.1103/PhysRevLett.92.073002

PACS numbers: 31.70.-f, 33.80.Gj

A basis of quantum chemistry is the Born-Oppenheimer (BO) approximation, according to which nuclei move on single adiabatic potential energy surfaces created by the much faster moving electrons. This approximation permits one to define isolated electronic molecular states and their energy levels. Many interesting aspects of molecular dynamics such as molecule formation and dissociation arise from the breakdown of this approximation. This is due to small terms in the molecular Hamiltonian which originate from the finite response time of electron motion to changing nuclear position. They introduce couplings between the adiabatic states, whose integrated effect is observed in perturbations of the energy spectrum, and in ubiquitous examples of molecular dynamics such as dissociation, quenching, charge transfer, and spin-changing reactions [1]. A direct access to the dependence of these couplings on molecular coordinates has eluded experimental observation to date, except for diatomics [2].

We show here that the quantum mechanical coupling, which leads to dissociation, emerges as a distinct map in the correlation of fragment momentum vectors in the reaction



We monitor this reaction for individual, state-selected H_3^* molecules and determine the three atomic momentum vectors in coincidence using the technology described previously [3–5]. The decay channel in reaction (1) and the competing process of autoionization of H_3^* control the rate of electron capture of H_3^+ , an important process in the interpretation of the density of H_3^+ in the diffuse interstellar medium [6,7].

In our experiment we prepare metastable triatomic hydrogen molecules in a fast (3 keV) beam by charge transfer neutralization of H_3^+ . The rotationless $2p^2A_2'$ state of H_3 is immune against rapid predissociation [8] and is present in the neutral beam in a range of vibrational levels $\{\nu_1, \nu_2\}$. In this notation ν_1 and ν_2 describe the symmetric stretch and degenerate bending mode vibrational quantum numbers. Photoexcitation spectra of H_3 and D_3 have been studied in detail [9] and firm electronic,

vibrational, and rotational assignments of the spectra have emerged, backed by the multichannel quantum defect theory based solely on *ab initio* parameters [10].

The molecules are photoexcited inside the cavity of a narrow band dye laser which is tuned to a specific absorption transition. In this way the total energy of the molecule, W , measured relative to three separated hydrogen atoms, $\text{H}(1s) + \text{H}(1s) + \text{H}(1s)$, is precisely defined in the experiment. This situation is indicated in Fig. 1, which gives a cut through the potential energy surfaces of H_3 along the symmetric stretch coordinate. The excited electronic states of H_3 and D_3 are embedded in the repulsive ground-state continuum which dissociates into the limits $\text{H}_2(^1\Sigma_g^+) + \text{H}(1s)$ or into the three-particle limit $\text{H}(1s) + \text{H}(1s) + \text{H}(1s)$. In the coordinate shown in Fig. 1 the seam of the Jahn-Teller intersection of the two sheets of the ground-state surfaces appears [11]. The fast H_3 molecules spend ≈ 3 ns in the laser interaction region. Following photoexcitation they typically predissociate on time scales of 1–10 ns [12], their center of mass propagating at an energy of 3 keV towards a detector. The photofragments separate spatially from this direction according to their transverse momentum. The fragments are detected in coincidence using position- and time-sensitive multihit

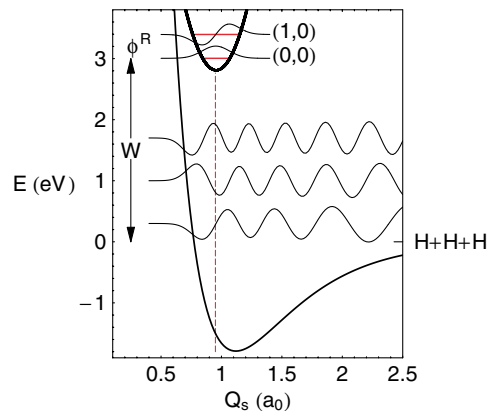


FIG. 1 (color online). Cut of potential energy surfaces of H_3 along the symmetric stretch coordinate (D_{3h} geometry). Bound state wave functions of the $3sA_1'$ state are shown together with three continuum functions of total energy W .

detectors [4] after a free flight of about 150 cm. Over this flight distance the fragments separate in space by as much as 100 mm. Fast electronic signal processing permits one to measure the spatial coordinates of their impact positions with a resolution of $<100 \mu\text{m}$ and their arrival time differences with a resolution of $<100 \text{ps}$. At the same time it triggers a triple-coincidence logic routine which examines the positions and arrival times to distinguish process (1) from fragmentation into $\text{H}_2(^1\Sigma_g^+) + \text{H}(1s)$ [13]. For each triple-coincidence event, the momentum vectors $\{\vec{k}_1, \vec{k}_2, \vec{k}_3\}$ in the center-of-mass frame are evaluated from the time and position information. After recording the dissociation of $\approx 10^4$ molecules, we obtain a map of preferred momentum correlation, under which the selected H_3^* state escapes into the three-particle continuum. These data are coded into a Dalitz plot (see below) after accounting for the geometric detection efficiency [5].

In this work we determined the correlation map for a variety of electronic and vibrational molecular states of H_3 and D_3 . Examples are shown in Figs. 2 and 3 for the lowest rotational energy levels in the electronic states of $3sA_1'$, $3dE''$, and $3pE'$ symmetry at varying degrees of vibrational excitation, $\{0, 0\}$, $\{0, 1\}$, and $\{1, 0\}$. The $3pE'$ state is populated by spontaneous emission from the laser-selected $3dE''$ state. Pronounced islands of high proba-

bility appear, their location depending on the type of electronic excitation, vibrational state, and nuclear mass. All states shown here lie close in energy ($W = 2.5\text{--}3.6 \text{eV}$); thus they probe similar regions of the ground-state energy surface. The initial electronic states have nearly identical nuclear geometry because the adiabatic potential energy surfaces of the excited states are all close to the geometry of the parent ion core H_3^+ [14]. The tightly bound ion is of D_{3h} geometry with a proton separation of $1.64a_0$ at the potential minimum. The attached Rydberg electron adds small modifications to the binding, leading to small ($<5\%$) variations in the proton separation at equilibrium. However, the electronic, rovibrational, and nuclear symmetries of the excited states differ and thereby control the coupling matrix elements for predissociation into the ground-state continuum. This feature dictates the appearance of the Dalitz plots as we discuss below.

The exit channel in reaction (1) is well-defined in terms of three plane waves with center-of-mass momenta \vec{k}_i . Neglecting spin and orbital angular momenta it may be written as the product wave function of the three hydrogen atoms,

$$\psi^c = \phi_1(\vec{k}_1)\phi_2(\vec{k}_2)\phi_3(\vec{k}_3). \quad (2)$$

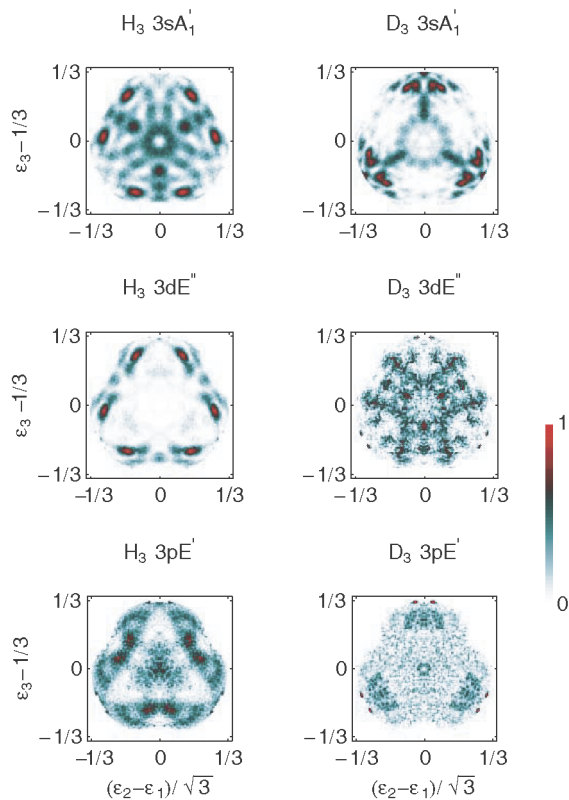


FIG. 2 (color online). Final state momentum correlation measured in three-body decay of the $3sA_1'$, $3dE''$, and $3pE'$ electronic states of H_3 (left) and D_3 (right).

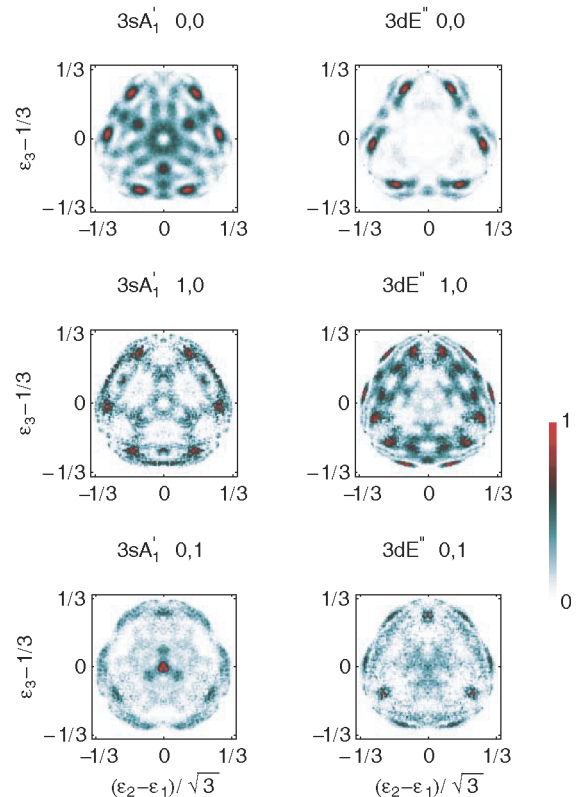


FIG. 3 (color online). Final state momentum correlation measured in three-body decay of the $3sA_1'$ and $3dE''$ electronic states of H_3 for different degrees of vibrational excitation $\{\nu_1, \nu_2\}$.

Since the molecular state under study is selected in the laser-excitation step the energy condition

$$W = \frac{1}{m} (|\vec{k}_1|^2 + |\vec{k}_2|^2 + |\vec{k}_3|^2) \quad (3)$$

holds (m being the hydrogen mass), in addition to momentum conservation $\vec{k}_1 + \vec{k}_2 + \vec{k}_3 = 0$. A unique map of three correlated momentum vectors can be represented in a Dalitz [15] plot. This probability-density plot gives the vector correlation in terms of the reduced energies of the three atoms,

$$\epsilon_3 - \frac{1}{3} \quad \text{vs} \quad \frac{\epsilon_1 - \epsilon_2}{\sqrt{3}}, \quad (4)$$

where $\epsilon_i = |\vec{k}_i|^2/(2mW)$. Figure 4 illustrates the meaning of the position of an event in the Dalitz plot in terms of the orientation and magnitude of the fragment momenta. Thus islands of preferred population in a Dalitz plot refer to specific orientations of final-state fragment momenta in the center-of-mass frame.

At present, no rigorous theory has treated a molecular three-body problem such as (1); however, a formal discussion can be given. The initially bound H_3^* molecule is prepared at time t_0 . At low vibrational excitation its heavy particle wave function $\psi^R(t_0)$ is restricted by locally quadratic potentials. It is characterized by products of harmonic oscillator wave functions χ in the symmetric stretch and bending normal mode coordinates, Q_s and Q_b , with $\{i, j\}$ quanta of vibrational excitation,

$$\psi_{i,j}^R(t_0) = \chi_i(Q_s)\chi_j(Q_b). \quad (5)$$

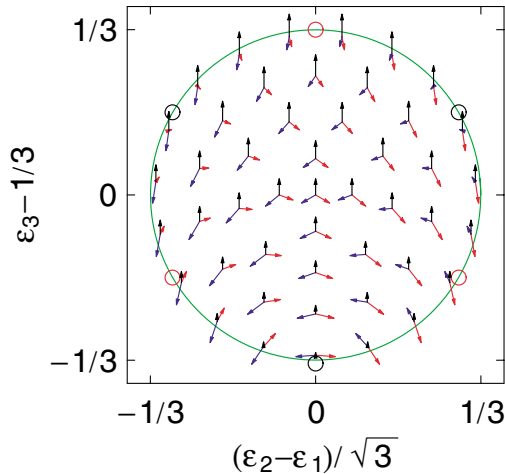


FIG. 4 (color online). Characteristic momentum vector orientations for specific points in the Dalitz plot. Note that in the Dalitz coordinates (4) all events are restricted by energy and momentum conservation to an area within a circle of radius $1/3$. For a homonuclear molecule a sixfold degeneracy appears. The three areas marked by circles at the azimuthal angles 0° , 120° , and 240° correspond to dissociation into $\text{H} + \text{H}_2$. The circles at 60° , 180° , and 300° mark where one hydrogen atom remains at rest in the center-of-mass frame.

In a time-dependent approach we may formally view process (1) as a sequence of two steps. In a first phase the bound molecular state accesses the repulsive ground-state surface of H_3 ,

$$\psi^m(t_1) = \mathcal{F}\psi_{i,j}^R(t_0), \quad (6)$$

where $\psi^m(t_1)$ is a continuum wave packet at molecular distances and the operator \mathcal{F} describes the modification of the normal mode wave functions due to the coupling. This phase is followed by the evolution of the wave packet on the continuum energy surface [16]

$$\psi^c(t) = \int_{t_1}^t dt' e^{i\mathcal{H}t'} \psi^m(t_1), \quad (7)$$

where \mathcal{H} is the Hamiltonian describing the motion of the three atoms. In the limit of $t \rightarrow \infty$ the function $\psi^c(t)$ approaches Eq. (2). Significant pieces of information required to carry out the propagation in (6) and (7) have been developed recently. Among these are studies of some of the nonadiabatic [17,18] and Jahn-Teller induced couplings [6] as well as time-dependent dynamics simulations [16–19].

To illustrate the meaning of our data we have modeled the process under the assumption that the continuum access in Eq. (6) is equally probable throughout the available phase space, i.e., $\mathcal{F} = 1$. This reduces the problem to propagation of the wave packet (5) on the ground-state surface. The three-particle channel is primarily populated [19] via the upper sheet of the Jahn-Teller split ground-state surface [11] and a wave packet motion on this surface is tightly confined near the D_{3h} geometry [17]. To predict the momentum vector correlation, we may in a first crude approximation consider the probability map

$$\mathcal{P}(\vec{k}_1, \vec{k}_2, \vec{k}_3) = |\langle \psi^c | \psi_{i,j}^R \rangle|^2 \quad (8)$$

with the restrictions imposed by energy and momentum conservation. We have solved Eq. (8) numerically using continuum Morse wave functions for ψ^c and harmonic oscillator wave functions for the bound molecular state $\psi_{i,j}^R$. Typical results are shown in Fig. 5 for H_3 and D_3 . The projection in Eq. (8) is between the bound state and the three continuum wave functions (see Fig. 1). Going from H_3 to D_3 the bound state wave function narrows and the spatial oscillation period of the continuum functions decreases. In the coordinates of the Dalitz plot this projection is evaluated for relative energies of the individual fragments ranging from $0 \leq \epsilon_i \leq 2W/3$. As a consequence undulations of the type of Condon-diffraction bands appear which move in the radial and azimuthal coordinate of the Dalitz plot as either the mass or the total energy W changes.

While our simple model fails to explain the finer details in the measured correlation maps, several modes of agreement can be pointed out. For the case of $D_3\{0,0\}$

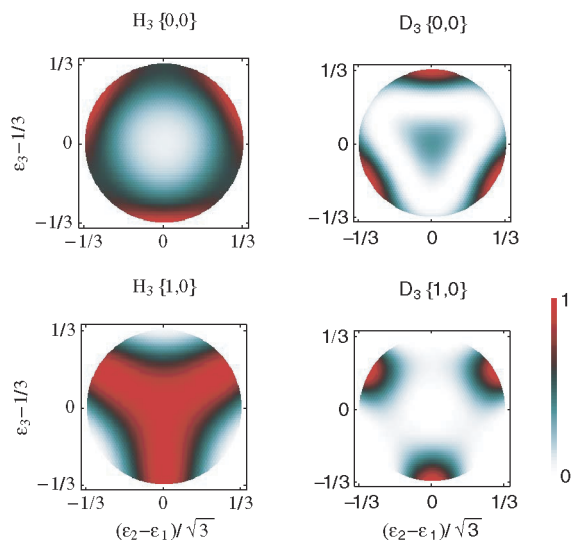


FIG. 5 (color online). Predictions of Eq. (8) for the vibrational ground state $\{0, 0\}$ and for the symmetric stretch excited state $\{1, 0\}$ for H_3 and D_3 at $W = 3.10$ eV.

our model predicts minimal population for the configurations where one of the fragments remains at rest in the center-of-mass frame (circles at 60° , 180° , and 300° in Fig. 4). This is indeed observed (see Fig. 2, right column). The opposite is true for $H_3\{1, 0\}$ for which maximal contributions are predicted in a triangle connecting these configurations. This again is in agreement with the observations (see Fig. 3, center row).

We attribute the failure of our model in predicting the fine structure of the Dalitz plots to the assumption that $\mathcal{F} = 1$. The projection of the wave packet in Eq. (6) depends sensitively on the overlap of the initial H_3^* state with the continuum and restrictions imposed on the projection by symmetry considerations. On the basis of symmetry arguments we know that predissociation of sA_1' states is mediated by the degenerate bending mode, predissociation of dE'' states is by rotational coupling [20], and predissociation of pE' states is by Jahn-Teller coupling [6]. The different coupling mechanisms imply that for each electronic state different areas of phase space play the leading role in step (6). Indeed the strongest variation in Figs. 2 and 3 is among maps of different electronic symmetry.

We therefore conclude that our experiment provides a direct image of the action of the operator \mathcal{F} , which couples excited molecular states with the final-state continuum. The dependence of \mathcal{F} on electronic and nuclear coordinates and symmetries is embedded in an inverse

problem of relating probability density in the Dalitz plot to phase-space density of the molecular level.

Since final and initial states are precisely defined in the experiment, the challenge is to perform a quantum calculation with a proper account of electronic and nuclear degrees of freedom. Theoretical insight into this subject will aid the interpretation of correlation maps obtained in non-state-specific experiments [7], the prediction of the correct capture rate of slow electrons by H_3^+ [6], and extend our basis for a microscopic understanding of nonadiabatic couplings. Certainly the experiment has reached a level of sophistication which warrants an in-depth confrontation with this fundamental system of three protons and three electrons.

This research was supported by TPC13 of the Sonderforschungsbereich 276 of the Deutsche Forschungsgemeinschaft. We acknowledge fruitful discussions with Professor J. S. Briggs, Professor M. Jungen, Dr. M. Walter, and Dr. A. Meremianin.

- [1] D. R. Yarkony, *J. Phys. Chem.* **100**, 18612 (1996).
- [2] H. Lefebvre-Brion and R.W. Field, *Perturbations in the Spectra of Diatomic Molecules* (Academic Press, Inc., Orlando, 1986).
- [3] U. Müller *et al.*, *Phys. Rev. Lett.* **83**, 2718 (1999).
- [4] M. Braun, M. Beckert, and U. Müller, *Rev. Sci. Instrum.* **71**, 4535 (2000).
- [5] U. Galster *et al.*, *Eur. Phys. J. D* **17**, 307 (2001).
- [6] V. Kokouline, C.H. Greene, and B.D. Esry, *Nature (London)* **412**, 891 (2001).
- [7] D. Strasser *et al.*, *Phys. Rev. A* **66**, 032719 (2002).
- [8] G.I. Gellene and R.F. Porter, *J. Chem. Phys.* **79**, 5975 (1983).
- [9] R. Reichle *et al.*, *Phys. Rev. A* **60**, 3929 (1999), and references therein.
- [10] I. Mistrík *et al.*, *Phys. Rev. A* **61**, 033410 (2000).
- [11] Y.-S. M. Wu, A. Kuppermann, and J. B. Anderson, *Phys. Chem. Chem. Phys.* **1**, 929 (1999).
- [12] I. Mistrík *et al.*, *Phys. Rev. A* **63**, 042711 (2001).
- [13] M. Beckert and U. Müller, *Eur. Phys. J. D* **12**, 303 (2000).
- [14] I. D. Petsalakis, G. Theodorakopoulos, and J.S. Wright, *J. Chem. Phys.* **89**, 6850 (1988).
- [15] R. H. Dalitz, *Philos. Mag.* **44**, 1068 (1953).
- [16] J. L. Krause *et al.*, *J. Chem. Phys.* **96**, 4283 (1992).
- [17] S. Mahapatra and H. Koepfel, *J. Chem. Phys.* **109**, 1721 (1998).
- [18] I. F. Schneider and A. E. Orel, *J. Chem. Phys.* **111**, 5873 (1999).
- [19] A. E. Orel and K.C. Kulander, *J. Chem. Phys.* **91**, 6086 (1989).
- [20] U. Müller and P.C. Cosby, *Phys. Rev. A* **59**, 3632 (1998).